RSC Advances

PAPER

View Article Online
View Journal | View Issue

Cite this: *RSC Adv.*, 2024, **14**, 28753

Glycyrrhetinic acid-modified redox-sensitive polymeric mixed micelles for tumor-specific intracellular delivery of cantharidin†

Yu Hu,[a] Tian Lan,[b] Ji Li,[c] Lingjun Li‡*[a] and Jizheng Song ‡*[a]

Cantharidin (CTD) has been widely used to treat hepatocellular carcinoma (HCC) in clinical practice. However, the current CTD preparations may induce hepatic and renal damage due to their non-specific distribution. Therefore, redox-sensitive polymer Pluronic F127-disulfide bond-poly(D,L-lactide) (F127-SS-PDLA) and active targeting polymer F127-glycyrrhetinic acid (F127-GA) were synthesized to prepare mixed micelles (GA/F127-SS-PDLA/CTD) for effective delivery of CTD. Fourier transform infrared (FTIR) spectroscopy and ^{1}H nuclear magnetic resonance (^{1}H-NMR) spectroscopy were used to verify the successful synthesis of F127-SS-PDLA and F127-GA. During the preparation, this study was the first to screen the density of GA by cellular uptake assay. The results indicated that mixed micelles with 10% and 15% F127-GA (weight fraction) exhibited superior cellular uptake in comparison to micelles with 5% and 20% F127-GA. GA/F127-SS-PDLA/CTD micelles prepared by thin film hydration method demonstrated excellent drug loading capacity for CTD (16.12 ± 0.11%). The particle size and zeta potential of GA/F127-SS-PDLA/CTD micelles were 85.17 ± 1.24 nm and −11.71 ± 0.86 mV, respectively. Hemolysis and stability assay showed that the mixed micelles had good blood compatibility and could remain stable for 30 days at 4 °C. The redox-sensitivity of GA/F127-SS-PDLA/CTD micelles *in vitro* was verified under reducing conditions through dynamic light scattering (DLS) and an *in vitro* drug release experiment, which showed obvious particle size variation and rapid drug release ability. In cellular experiments, GA/F127-SS-PDLA/CTD micelles could induce superior cytotoxicity, apoptosis and intracellular reactive oxygen species (ROS) levels compared with free CTD, non-sensitive F127-PDLA/CTD micelles and redox-sensitive F127-SS-PDLA/CTD micelles. The cellular uptake ability of nile red-labeled GA/F127-SS-PDLA micelles, which was evaluated *via* fluorescent microscope and flow cytometry, indicated that the modification of GA significantly increased micelle uptake in HepG-2 cells. Consequently, GA/F127-SS-PDLA/CTD micelles could be considered as a satisfactory drug administration strategy in the treatment of HCC.

Received 29th April 2024
Accepted 31st August 2024

DOI: 10.1039/d4ra03171g

rsc.li/rsc-advances

1 Introduction

Hepatocellular carcinoma (HCC) is the sixth commonest form of cancer and the second leading cause of cancer-associated death worldwide.[1] Since HCC is asymptomatic in its early stage, most interventions, such as liver transplantation and hepatectomy, are often limited by cancer recurrence and metastasis.[2] As a result, chemotherapy is currently a commonly used and effective treatment for HCC in clinical practice.[3,4]

Cantharidin (CTD) is a sesquiterpenoid derivative extracted from the *Mylabris*.[5,6] It is famous for its remarkable and widespread anti-tumor effects.[6–8] Modern pharmacological research has shown that the anti-tumor mechanism of CTD primarily involved suppressing tumor cell growth, inducing tumor cell apoptosis and blocking the tumor cell cycle.[9,10] Various preparations containing CTD and its derivatives are widely used in treating HCC, such as aidi injection, disodium cantharidinate injection and compound CTD capsule.[2,11,12] These preparations can significantly relieve the symptoms of patients and prolong their survival time. However, CTD preparations might cause liver and kidney damage in the long term, which could be attributed to the nonspecific distribution of CTD.[13–15] Therefore, it is crucial to establish a novel targeting drug delivery system, which could decrease the side effects and toxicity of the drugs, enhance the anti-tumor effect and expand the scope of CTD.

Nanodrugs have shown great potential in cancer treatment. They can aggregate in tumor tissue through the high permeability and retention effect of solid tumors (EPR effect) by virtue

[a]*School of Pharmacy, Shandong University of Traditional Chinese Medicine (TCM), 250355 Jinan, Shandong, China. E-mail: sdzyylilingjun@163.com; songjizheng345@163.com*

[b]*Innovative Institute of Chinese Medicine, Shandong University of TCM, 250355 Jinan, Shandong, China*

[c]*Affiliated Hospital of Shandong University of TCM, 250011 Jinan, Shandong, China*

† Electronic supplementary information (ESI) available. See DOI: https://doi.org/10.1039/d4ra03171g

‡ These authors contributed equally to this work and should be considered as corresponding author.

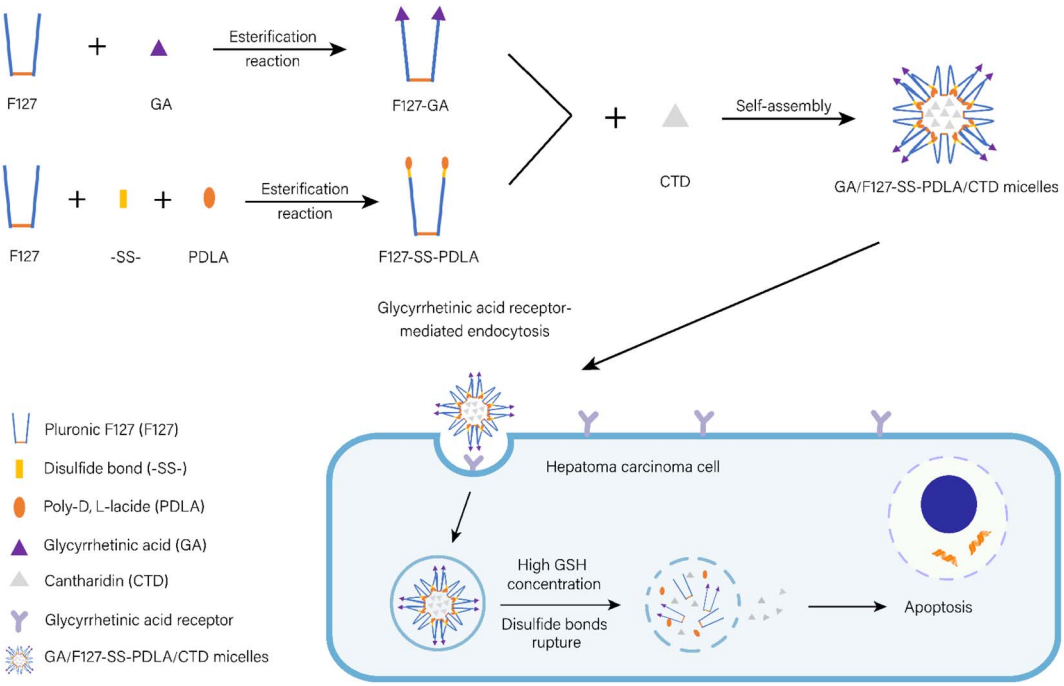

Fig. 1 The preparation of GA/F127-SS-PDLA/CTD micelles which were targeted to hepatoma carcinoma cell and released CTD responding to the reducing environment within cell to increase the cellular apoptosis.

of their small sizes (10–200 nm).[16] In aqueous solution, amphiphilic block copolymers are able to self-assemble into polymeric micelles with "core–shell" structure.[17] At present, micelles loaded with chemotherapy drugs such as paclitaxel and docetaxel have been approved for clinical use.[18,19] These agents have exhibited higher overall response rates and greater safety profiles compared with conventional chemotherapeutic drugs. As reported in the literature, micelles have been used to deliver CTD.[5] However, conventional nanoparticles may encounter challenge in incomplete drug release.[20,21] The disulfide bond is responsive to the reductive environment. It can cleave rapidly at high concentrations of glutathione (GSH) in tumor cells while remaining stable in normal tissues and blood.[22] At present, it has been widely used in the development of anti-tumor drug delivery carriers and exerted superior efficacy.[23,24] Nevertheless, the utilization of redox-sensitive formulations for intracellular delivery of CTD has yet to be reported in detail.

An ideal drug delivery carrier should not only trigger the rapid release of drugs under specific stimulation conditions but also exhibit excellent biocompatibility and drug loading capacity.[25] Therefore, due to their exceptional physical and biological properties, polymeric materials have become the potential candidates for establishing stimulus-responsive nanocarriers. Pluronic F127 (F127), a triblock copolymer, has been recognized as an excipient by British Pharmacopoeia for intravenous injection.[26] Using F127 to prepare micelles could improve the solubility of drugs and target drugs to the tumor site passively.[27] Nevertheless, the high critical micelle concentration (CMC) of F127 limited its clinical application.[26] Given this circumstance, the hydrophobic poly(D,L-lactide) (PDLA) with good degradability and biocompatibility could be used to modify F127 to increase the hydrophobicity of F127 and subsequently enhance the stability and anti-dilution property of micelles.[28]

Although passive targeting agents can deliver drugs to the tumor tissue through the EPR effect, they still need more specificity towards tumor cells.[29,30] Therefore, it is significant to design nanoparticles with active targeting ability to deliver drugs to tumor cells precisely.[31] Glycyrrhetinic acid (GA) receptors are overexpressed on the surface of liver cancer cells, which can specifically recognize and bind with GA.[21,32] Therefore, drug delivery carriers modified with GA can minimize non-specific interactions with normal tissues and improve the anti-tumor effect of the drug.[21,33] Furthermore, the density of the targeting ligands plays a crucial role in the targeting ability of drug delivery carriers.[34] The inappropriate density of ligands may weaken the targeting capacity of nanoparticles.[35] However, most reported active targeting nano-preparations have not been screened for the suitable density of targeting ligands particularly GA.

In this study, a CTD-loaded active targeting and reduction-sensitive mixed micelles composed of F127-disulfide bond-PDLA (F127-SS-PDLA) and F127-GA were established for HCC treatment (Fig. 1). Firstly, the disulfide bond was used to connect F127 and PDLA to synthesize F127-SS-PDLA. F127 was esterized with GA to obtain F127-GA. Secondly, in order to further improve the active targeting efficiency of the micelles, the appropriate proportion of F127-GA in the mixed micelle system was explored by cellular uptake assay. Thirdly, CTD-loaded mixed micelles F127-GA/F127-SS-PDLA/CTD (GA/F127-SS-PDLA/CTD) were then formulated by self-assembly of two

polymers and characterized by particle size, polydispersity index (PDI), zeta potential, encapsulation efficiency (EE), drug loading (DL) and stability. Meanwhile, to evaluate the redox-sensitive function of the preparation, a non-sensitive polymer material, F127-PDLA, was synthesized and served as the control group of F127-SS-PDLA in the *in vitro* drug release assay and cell experiments. Finally, the inhibitory effect of GA/F127-SS-PDLA/CTD micelles on human hepatocellular carcinoma cells HepG-2 was investigated by cytotoxicity assay, apoptosis assay, reactive oxygen species (ROS) levels detection and cell uptake assay.

2 Materials and methods

2.1 Materials and chemicals

GA was purchased from J&K Scientific Co., Ltd (Beijing, China). F127 (average molecule weight = 14 600), anhydrous dichloromethane, *N*-(3-dimethylaminopropyl)-*N*′-ethylcarbodiimide hydrochloride (EDC), 4-dimethylaminopyridine (DMAP) and CTD were supplied by Aladdin Biotechnology Co., Ltd (Shanghai, China). 3,3′-Dithiodipropionic (SS-COOH) was purchased from Yuanye Biotechnology Co., Ltd (Shanghai, China). *P*-toluenesulfonic acid (*p*-TSA) was obtained from Shanghai Macklin Biochemical Co., Ltd (Shanghai, China). PDLA (average molecular weight = 4700) was bought from Jinan Daigang Biological Engineering Co., Ltd (Jinan, China). *N*,*N*-dimethylformamide (DMF), triethylamine (TEA) and other chemical reagents were from Sinopharm Chemical Reagent Co., Ltd (Shanghai, China).

Dulbecco's Modified Eagle's Medium (DMEM), fetal bovine serum (FBS), penicillin streptomycin (P/S), 0.25% trypsin-EDTA were provided by Gibco. 3-(4,5-Dimethyl-2-thiazolyl)-2,5-diphenyl-tetrazolium bromide (MTT) was obtained from Beijing Solarbio Technology Co., Ltd (Beijing, China). Annexin V-FITC/propidium iodide (PI) assay kit, ROS assay kit and Hoechst 33 342 were supplied by Servicebio Biotechnology Co., Ltd (Wuhan, China). Phosphate buffered saline (PBS) and trypsin solution (free EDTA) were obtained from Biosharp Biotechnology Co., Ltd.

2.2 Cells culture

HepG-2 cell line was acquired from Shanghai Anwei Biotechnology Co., Ltd (Shanghai, China) and cultured with DMEM containing 10% FBS (v/v) and 1% P/S (v/v) under 37 °C in a humidified atmosphere containing 5% CO_2.

2.3 Synthesis of polymer materials

2.3.1 Synthesis of F127-GA. The F127-GA polymer was synthesized through an esterification reaction according to our previous report (Fig. 2A).[21] Briefly, F127 0.1 mmol, GA 0.3 mmol, EDC 0.3 mmol, DMAP 0.3 mmol and TEA 0.3 mmol were dissolved in 10 mL of anhydrous dichloromethane and stirred at room temperature for 24 h. After removing the dichloromethane by the N-1300 rotary evaporator (EYELA, Tokyo, Japan), the residues were redissolved in 10 mL of acetone and dialyzed against water in a dialysis bag with molecular weight cutoff (MWCO) at 5000 Da for 24 h to remove acetone and unreacted substances. After centrifugation at 5000 rpm for 10 min to remove the precipitate, F127-GA was finally harvested by lyophilization using the Xinzhi SCIENTZ-10N freezer dryer (Zhejiang, China) and preserved at 4 °C.

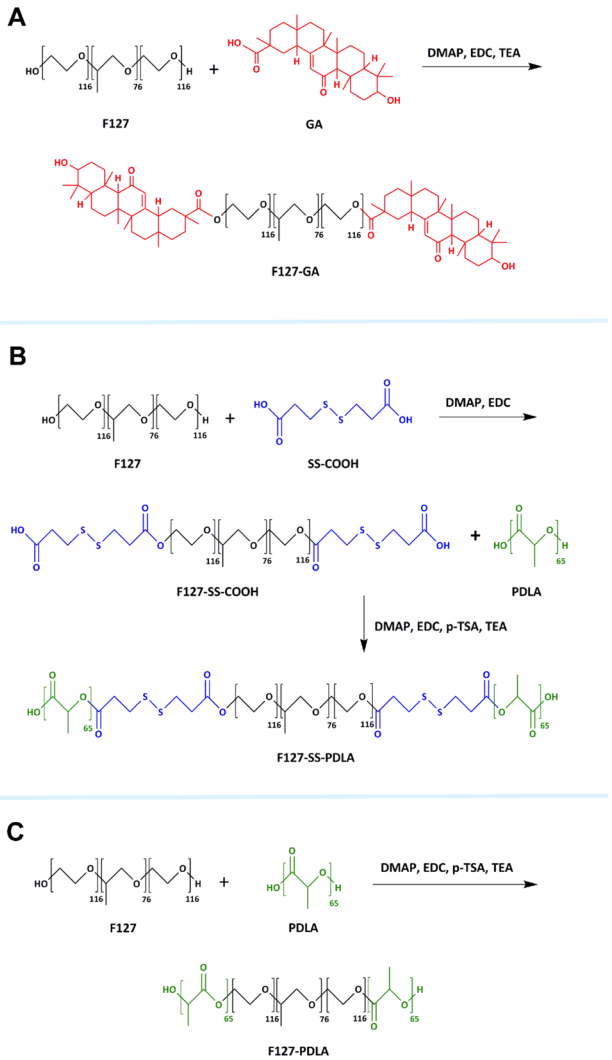

Fig. 2 The synthesis routes of (A) F127-GA, (B) F127-SS-PDLA and (C) F127-PDLA.

2.3.2 Synthesis of F127-SS-PDLA. The synthesis of redox-sensitive polymer F127-SS-PDLA was achieved by two-step esterification reactions (Fig. 2B). Firstly, F127-SS-COOH was obtained by the conjugation of F127 with SS-COOH. In brief, F127 0.05 mmol, SS-COOH 0.12 mmol and DMAP 0.04 mmol were dissolved in 10 mL DMF. The mixture was stirred well and activated at 0 °C for 3 h. Then, EDC 0.05 mmol was added and the reaction was continued for 24 h. The resultant solution was purified using a dialysis bag (MWCO = 5000 Da) and dialyzed against water for 24 h to remove DMF and the excess SS-COOH, DMAP and EDC. F127-SS-COOH was finally obtained by lyophilization. Secondly, PDLA was modified to the terminal of F127-SS-COOH to synthesize F127-SS-PDLA. In short, F127-SS-COOH 0.05 mmol, DMAP 0.08 mmol, EDC 0.10 mmol and *p*-TSA 0.10 mmol were dissolved in 10 mL DMF and stirred well at 0 °C

for 4 h. Then, PDLA 0.12 mmol and TEA 0.10 mmol were added. After 24 h of reaction at room temperature, the reaction mixture was loaded into a dialysis bag (MWCO = 5000 Da) and dialyzed exhaustively for 24 h to remove unreacted raw materials and DMF. After centrifugation to remove the unreacted PDLA, the supernatant was taken. F127-SS-PDLA was finally obtained by freeze-drying and preserved at 4 °C for use.

2.3.3 Synthesis of F127-PDLA. Non-sensitive polymeric material F127-PDLA was obtained by conjugating PDLA to F127 *via* an esterification reaction. The synthesis route was shown in Fig. 2C. Briefly, PDLA 0.12 mmol, DMAP 0.08 mmol, EDC 0.10 mmol and *p*-TSA 0.10 mmol were dissolved in 10 mL DMF and stirred well at 0 °C for 4 h. Then, F127 0.05 mmol and TEA 0.1 mmol were successively added and the mixture was reacted at room temperature for 24 h. The resultant solution was dialyzed for 24 h. F127-PDLA was finally obtained by centrifugation and lyophilization and stored at 4 °C for use.

2.4 Characterization of polymer materials

The structures of F127-GA, F127-SS-PDLA and F127-PDLA were confirmed by Fourier transform infrared (FTIR) spectroscopy (PerkinElmer Inc., USA). The polymers and potassium bromide powder in a dry state were thoroughly blended together before being compacted into a thin sheet. Then, the composites were analyzed with FTIR in the range of 4000 to 400 cm^{-1}. In addition, the structures were further identified with ADVANCE III HD-600 MHz nuclear magnetic resonance (^{1}H-NMR) spectroscopy (Bruker, Karlsruhe, Germany) with deuterated chloroform or deuterated dimethyl sulfoxide (DMSO) as the solvent.

2.5 Studying the proportion of F127-GA in the mixed micelle system

The proportion of targeting ligands in carrier materials had a significant impact on the targeting efficiency of the nanoparticles. For the purpose of screening the appropriate proportion of F127-GA in GA/F127-SS-PDLA/CTD micelles, the uptake ability of HepG-2 cells to various mixed micelles was investigated. Hydrophobic fluorescence probe, nile red (NR), was selected to use in this study. GA/F127-SS-PDLA/NR micelles with F127-GA proportion of 0%, 5%, 10%, 15% and 20% (weight fraction) were prepared for use.

2.5.1 Using the fluorescent microscope to study the cellular uptake. We seeded HepG-2 cells (130 000 cells per well) in a 12-well plate with 1 mL DMEM medium and cultured for 24 h. Then, a novel medium comprising micelles loaded NR (equivalent concentration of 0.3 μg mL^{-1} NR) was introduced and incubated for 4 h. After washed three times with PBS, the cells were fixed by 4% formalin for 10 min. Subsequently, the formalin was substituted with 1 mL Hoechst 33 342 (1 μg mL^{-1}) and the staining was performed for 5 min. After absorbing the Hoechst 33 342 solution, the cells were rinsed twice using PBS, then covered with 0.5 mL of PBS and photographed with the BZ-X810 fluorescent microscope (KEYENCE Ltd, Japan).

2.5.2 Using the flow cytometer to study the cellular uptake. Simultaneously, we also assayed the cellular uptake using the flow cytometer. We seeded HepG-2 cells (130 000 cells per well) in 12-well plates and incubated for 24 h. The cells were then incubated for 4 h with the novel medium containing various GA/F127-SS-PDLA/NR micelles (equivalent concentration of 0.3 μg mL^{-1} NR) instead of the original medium. After eliminating the medium, the cells were cleaned three times with PBS. The cells were collected by digestion and subjected to centrifugation. Subsequently, the precipitations were resuspended in PBS. The intensity of red fluorescence, reflecting the intracellular micelles, was detected by the PE channel of the Novo Ctye Advanteon flow cytometer (Agilent Ltd, USA).

2.6 Preparation of CTD-loaded micelles

Non-sensitive micelles F127-PDLA/CTD and reduction-sensitive micelles F127-SS-PDLA/CTD were prepared according to previously reported method.[21] Firstly, polymer materials (10 mg) and CTD (2 mg) were completely dissolved in acetone (5 mL). After removing acetone by rotary evaporation at 50 °C, −0.1 Mpa, 100 rpm, a transparent film was formed at the bottom of the eggplant-shaped bottle. Then, 10 mL of normal saline at the same temperature was added and hydrated at 50 °C for 30 min. The solution was cooled to room temperature, and the volume was diluted to a constant volume of 10 mL. The final F127-PDLA/CTD and F127-SS-PDLA/CTD micelles were obtained by filtering through 0.22 μm microporous membrane.

A total of 10 mg of F127-GA and F127-SS-PDLA were weighed at a ratio of 10 : 90 (w/w), and then GA/F127-SS-PDLA/CTD micelles were prepared as the method described above.

2.7 Characterization of CTD-loaded micelles

90Plus PALS dynamic light scattering (DLS, Brookhaven, USA) was used to determine the particles size and zeta potential of CTD-loaded micelles. The morphology of CTD-loaded micelles was observed and photographed by JEM 1400 Plus transmission electron microscopy (TEM, JEOL Ltd, Japan). The DL and EE of CTD-loaded micelles were determined by Agilent series 1260 high-performance liquid chromatography (HPLC) (Agilent Technologies, USA) equipped with a UV-vis detector set at 218 nm. The mobile phase was methanol/water (65/35, v/v) and the flow rate was 1 mL min^{-1}. Methanol was added to the micellar solution to destroy the micelle shells. The formulas provided below were utilized to calculate the DL and EE of CTD-loaded micelles:

$$\mathrm{DL}\ (\%) = M_a/(M_a + M_b) \times 100\%$$

$$\mathrm{EE}\ (\%) = M_a/M_c \times 100\%$$

where M_a, M_b and M_c represented the weight of CTD in micelles, the weight of carrier materials used to prepare the micelles and the weight of total added CTD, respectively.

2.8 The stability of CTD-loaded micelles

F127-SS-PDLA/CTD and GA/F127-SS-PDLA/CTD micelles were stored at 4 °C for 30 days, and their particle size and PDI were measured by DLS at predetermined time intervals (1, 3, 5, 10, 15, 20 and 30 days).

In addition, the particle size changes of CTD-loaded micelles in normal saline with 10% FBS were also investigated to preliminarily evaluate the ability of micelles to maintain their original state when exposed to plasma proteins. Briefly, F127-SS-PDLA/CTD and GA/F127-SS-PDLA/CTD micelles were exposed to 10% FBS and shaken at 100 rpm in 37 °C. At the scheduled time intervals (0, 1, 2, 4, 8, 12 and 24 h), the particle size of micelles was detected using DLS.

2.9 Reduction-responsive behaviour of CTD-loaded micelles

The particle size changes of micelles in 10 mM GSH solution were measured to assess the redox-triggered behaviour of CTD-loaded micelles. In brief, 2 mL of normal saline containing 20 mM GSH was added to 2 mL of F127-SS-PDLA/CTD and GA/F127-SS-PDLA/CTD micelles, respectively, to obtain the desired concentration of GSH. All of the mixture solutions were shaken at 100 rpm in 37 °C for 24 h. The size distributions of F127-SS-PDLA/CTD and GA/F127-SS-PDLA/CTD micelles were monitored by DLS at predetermined time points 0, 1, 2, 4, 8, 12 and 24 h.

2.10 *In vitro* drug release

The redox-triggered release of CTD from micelles was estimated through dialysis method. Appropriate amount of F127-PDLA/CTD, F127-SS-PDLA/CTD, GA/F127-SS-PDLA/CTD micelles and free CTD solutions were loaded in dialysis bags (MWCO = 5000), respectively. The dialysis bags were completely immersed in normal saline with different GSH concentrations (0 and 10 mM) and shaken at 100 rpm in 37 °C for 24 h. During this time, 1 mL of sample was collected at specified time intervals (0.25, 0.5, 1, 2, 4, 6, 8, 12 and 24 h) and 1 mL of fresh release medium at the same temperature was added. The amount of released CTD was measured by HPLC. Finally, the *in vitro* cumulative release curves of free CTD and three CTD-loaded micelles in different release media were plotted with the time and cumulative release rate as the abscissa and ordinate, respectively.

2.11 Hemolysis assay

The blood compatibility of blank F127-PDLA, F127-SS-PDLA and GA/F127-SS-PDLA micelles was preliminarily assessed by performing the hemolysis assay using red blood cells (RBCs).[21,26] Briefly, the RBCs separated from the whole blood of rat were collected by centrifugation. 2% Erythrocyte suspension (v/v) was obtained by cleaning and diluting RBCs utilizing normal saline. Then, 2 mL of erythrocyte suspension was interacted with 2 mL of blank micelles at varying concentrations. After shaken for 3 h in 37 °C at 100 rpm, the supernatant was collected *via* centrifugation. A microplate reader (CLARIOstar Plus, BMG Labtech, Germany) was utilized to determine the absorbance of the supernatant at 540 nm. The normal saline and distilled water were served as the negative and positive controls, respectively. The hemolysis rate was calculated based on the following equations:

$$\text{Hemolysis rate (\%)} = (A_1 - A_2) / (A_3 - A_2) \times 100\%$$

where A_1, A_2 and A_3 were the absorbance values of the sample, negative control and positive control, respectively.

2.12 Cytotoxicity assay

The MTT assay was employed to measure the *in vitro* cytotoxicity of free CTD, F127-PDLA/CTD, F127-SS-PDLA/CTD, GA/F127-SS-PDLA/CTD, blank F127-PDLA, blank F127-SS-PDLA and blank GA/F127-SS-PDLA micelles against HepG-2 cells. These findings are crucial for understanding the potential cytotoxicity of the micelles. HepG-2 cells (12 000 cells per well) were seeded in 96-well plates in 100 μL DMEM medium and incubated for 24 h. Then, we investigated the cells treated with free CTD, F127-PDLA/CTD, F127-SS-PDLA/CTD and GA/F127-SS-PDLA/CTD micelles at different concentrations ranging from 0.5 to 32.0 μg mL^{-1}, respectively. Meanwhile, the cells treated with blank F127-PDLA, blank F127-SS-PDLA and blank GA/F127-SS-PDLA micelles (3.125–200 μg mL^{-1}) were also investigated for the cytotoxicity of polymers. After incubating for 12 or 24 h at 37 °C, the previous solution was replaced with fresh DMEM medium that contained MTT (1 mg mL^{-1}). Then, the medium containing MTT was completely discarded after 4 h and each well received 150 μL of DMSO to dissolve the formazan crystal. The microplate reader measured absorbance values at 570 nm. Cells without treatment were served as control. The cell viability was calculated according to the following equation:

$$\text{Cell viability (\%)} = (OD_1/OD_2) \times 100\%$$

where OD_1 and OD_2 represented the absorbance values of sample and control wells, respectively.

2.13 Apoptosis assay

FITC-labelled Annexin-V was used to identify apoptotic cells that exposed phosphatidylserine (PS) to the outer leaflet. The cells with damaged membranes could also be stained with PI. Thus, flow cytometry was employed to quantify the apoptotic cells induced by various treatments through Annexin V-FITC/PI double staining. HepG-2 cells (250 000 cells per well) were placed in 6-well plates and cultured for 24 h. After treated with free CTD, F127-PDLA/CTD, F127-SS-PDLA/CTD and GA/F127-SS-PDLA/CTD micelles (equivalent concentration of 2.0 and 4.0 μg mL^{-1} CTD) for 12 h, the cells were harvested and subjected to centrifugation, then cleaned using PBS. The cell precipitates were resuspended with 0.5 mL of binding buffer (Annexin V-FITC 5.0 μL) and stained the PS for 15 min in darkness. In the end, 5.0 μL of PI was added to stain the nuclei and the mixture were evaluated by the flow cytometer.

2.14 Studying the effect of CTD-loaded micelles on ROS in HepG-2 cells

We detected the generation of intracellular ROS using a specific staining method with 2′,7′-dichlorodihydrofluorescein diacetate (DCFH-DA). This compound is able to penetrate the cell membrane and be intracellularly cleaved by esterase, resulting in the formation of 2′,7′-dichlorodihydrofluorescein (DCFH). ROS further oxidizes DCFH to form dichlorofluorescein (DCF)

emitting green fluorescence.[21] We seeded HepG-2 cells (130 000 cells per well) in a 12-well plate with DMEM medium and incubated them for 24 h. Then, the cells were treated with free CTD, F127-PDLA/CTD, F127-SS-PDLA/CTD and GA/F127-SS-PDLA/CTD micelles (equivalent concentration of 2.0 μg mL^{-1} CTD), respectively. After a 12 hours incubation, the cells were stained with DCFH-DA (10 μM) for 30 min. Finally, cells were collected by digestion as well as washed and resuspended with PBS. The intensity of green fluorescence, reflecting the intracellular ROS, was determined by the FITC channel of the flow cytometer.

2.15 Cellular uptake assay

For the sake of researching the internalization of mixed micelles within HepG-2 cells, we prepared different micelles labelled with NR using the thin film hydration method described above. Fluorescent microscope and flow cytometry were employed to assay the cellular uptake ability of F127-PDLA/NR, F127-SS-PDLA/NR and GA/F127-SS-PDLA/NR by HepG-2 cells. The experimental methods were referred to the content of 2.4.

2.16 Statistical analysis

All the experiments were conducted three times. Results were presented as mean ± standard deviation (SD). The statistical analysis was carried out by GraphPad Prism 8.3.0 and Origin 8.0 software. Statistical comparison was analyzed by *t*-test.

3 Results and discussion

3.1 Characterization of polymer materials

3.1.1 FTIR. FTIR spectroscopy was employed to preliminarily confirm the structure of F127-GA, F127-SS-COOH, F127-SS-PDLA and F127-PDLA.

The FTIR spectra of F127, GA, and F127-GA were shown in Fig. 3A. In the spectrum of GA, the stretching vibration absorption peak of C=O forming a p–π conjugate with C=C was at 1669 cm^{-1}. The absorption band of carboxyl group in GA was at 1708 cm^{-1}. Compared with F127 and GA, F127-GA retained the stretching vibration absorption peaks of C–O and C=O at 1116 cm^{-1} and 1669 cm^{-1}, respectively. Meanwhile, the absorption band of carboxyl group in GA (1708 cm^{-1}) disappeared. These changes were attributed to the formation of the ester group between GA and F127.

Fig. 3B displayed the FTIR spectra of polymer F127-SS-PDLA as well as its raw materials and intermediate. Compared with the spectra of F127, F127-SS-COOH retained the intrinsic absorption peaks of F127 at 2888 cm^{-1} and 1116 cm^{-1}, and added two stretching vibration absorption bands of C=O at 1700 cm^{-1} and 1734 cm^{-1}, respectively. The former was assigned to the terminal carboxyl group of F127-SS-COOH, and the latter was attributed to the ester bond. Combined with the spectrum of SS-COOH, the intermediate F127-SS-COOH was confirmed to be synthesized successfully. As shown in the FTIR spectrum of F127-SS-PDLA, a new peak belonging to PDLA arisen at 1760 cm^{-1}, manifesting that F127-SS-PDLA was successfully synthesized.

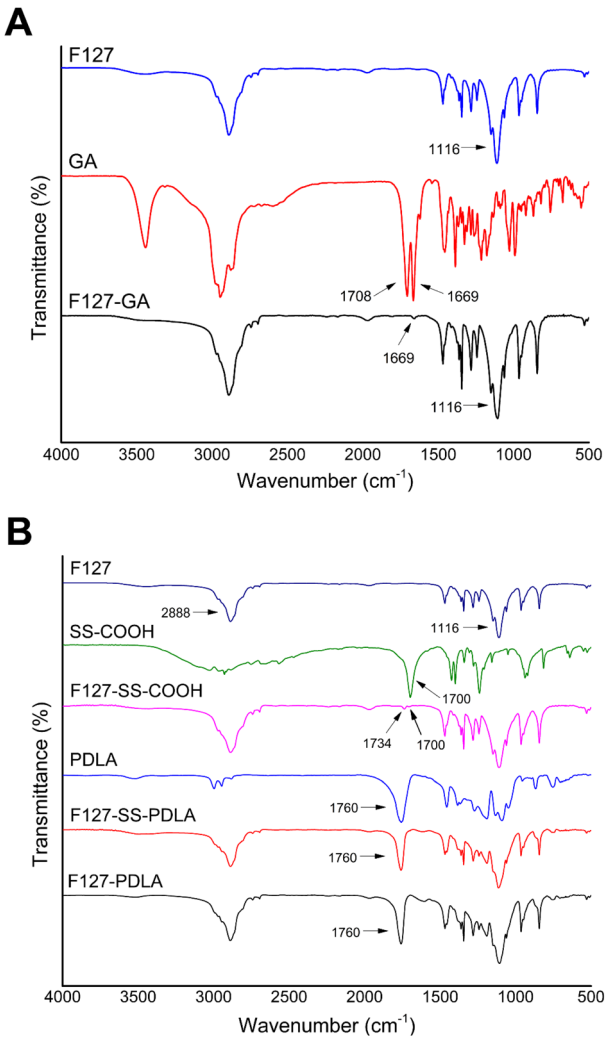

Fig. 3 The FTIR spectra of (A) F127-GA, (B) F127-SS-PDLA and F127-PDLA.

In the spectrum of F127-PDLA (Fig. 3B), the peaks at 2888, 1116 and 1760 cm^{-1} were responsible for stretching vibration of C–H, C–O in F127 and C=O in PDLA, inferring that F127-PDLA was synthesized successfully.

3.1.2 ^{1}H-NMR. Polymer materials F127-GA, F127-SS-PDLA and F127-PDLA were further validated by ^{1}H-NMR spectroscopy and their spectra were illustrated in Fig. 4.

The following characteristic peaks could be observed in the ^{1}H-NMR spectrum of F127. Peaks a (δ = 3.63 ppm) and b (δ = 3.52 ppm) were assigned to CH_2 in poly(ethylene oxide) (PEO) and poly(propylene oxide) (PPO), respectively. Peak c (δ = 3.39 ppm) and d (δ = 1.11 ppm) were the hydrogen signals of CH and CH_3 in PPO, respectively. As presented in the spectrum of GA, peak e (δ = 5.71 ppm) was attributed to alkene hydrogen in the steroidal nucleus. Peaks f (δ = 3.25 ppm) was the signal of hydrogen on the carbon linked to hydroxyl group of GA. Peaks g (δ = 2.77 ppm) and h (δ = 2.34 ppm) belonging to CH_2 in the steroidal nucleus. The signals between 0.70 and 2.00 ppm,

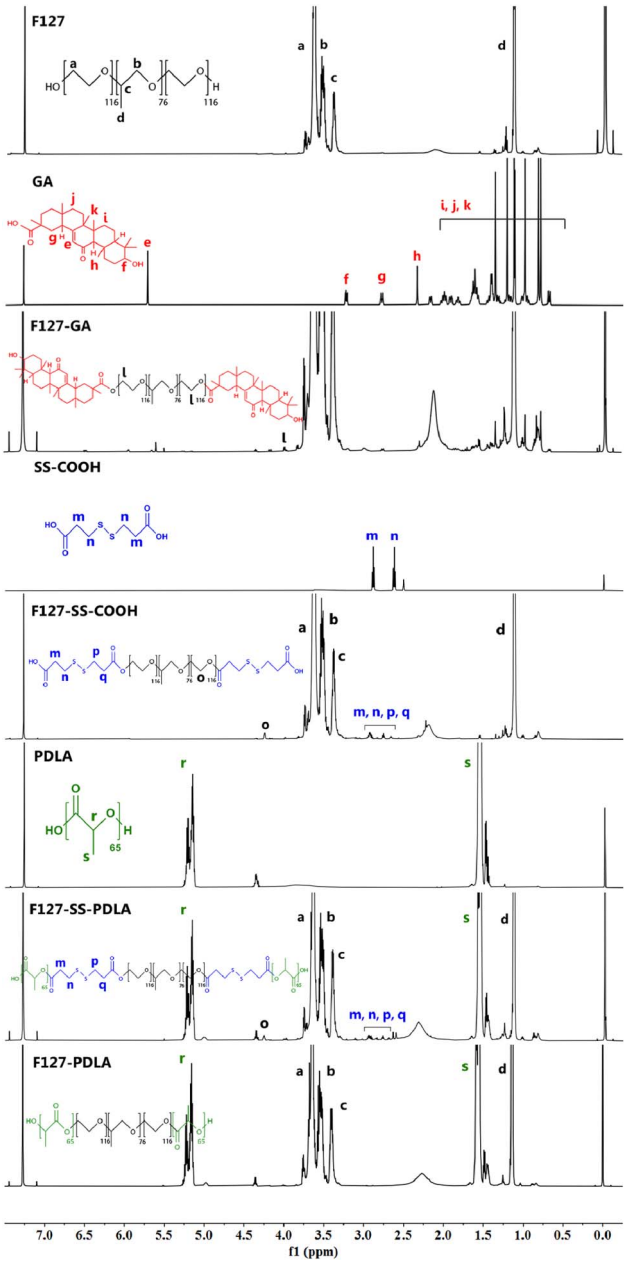

Fig. 4 The ^{1}H-NMR spectra of F127-GA, F127-SS-PDLA and F127-PDLA.

including peaks i, j and k, were assigned to the protons of saturated carbons. In addition to the typical signals of F127 and GA mentioned above, a new peak l (δ = 3.99 ppm) emerged in the spectrum of F127-GA, which possibly due to the change in chemical environment of CH_2 in the PEO after the formation of ester bond between F127 and GA. These data indicated that the carboxyl group of GA was successfully connected to the hydroxyl of F127.

In the ^{1}H-NMR spectrum of SS-COOH, peaks m (δ = 2.87 ppm) and n (δ = 2.62 ppm) were assigned to CH_2 on either side of the disulfide bond. As shown in the spectrum of F127-SS-COOH, peaks m and n became four peaks, including m, n, p and q (δ = 2.60–3.00 ppm). It was reasonable to refer that the ester group caused the change in the chemical environment of CH_2 in SS-COOH. Apart from the characteristic peaks of F127 and SS-COOH, a new peak o (δ = 4.24 ppm) appeared in the spectrum of F127-SS-COOH which may be caused by the changes in chemical environment of CH_2 in of PPO after the esterification reaction between F127 and SS-COOH. These results were indicated that the intermediate product F127-SS-COOH was synthesized successfully.

The ^{1}H-NMR spectra of PDLA and F127-SS-PDLA displayed the characteristic peaks of PDLA, including peaks r (δ = 5.18 ppm) and s (δ = 1.55 ppm) which corresponded to the CH and CH_3 in the PDLA, respectively. Furthermore, in the spectrum of F127-SS-PDLA, the characteristic peaks of F127-SS-COOH also appeared, implying the successful synthesis.

The specific signals of F127 and PDLA could be found simultaneously from the ^{1}H-NMR spectrum of F127-PDLA, indicating that F127-PDLA was synthesized successfully.

3.2 The appropriate proportion of F127-GA in the mixed micelle system

The results of the fluorescence microscopy imaging system and flow cytometry (Fig. 5) underscore the significance of our work. The red fluorescence intensity of GA/F127-SS-PDLA/NR micelles, with varying proportions of F127-GA, followed a distinct pattern: 10% F127-GA ≈ 15% F127-GA > 20% F127-GA > 5% F127-GA > 0% F127-GA. It was suggested that the introduction of GA could increase the uptake of micelles by HepG-2 cells and the binding affinity of mixed micelles with 10% and 15% F127-GA to HepG-2 cells was significantly higher than that of mixed micelles with 20% and 5% F127-GA.

Previous studies have demonstrated that the density of targeting ligands on the surface of drug delivery carriers significantly influenced the nanoparticle's targeting efficacy. The similarity of these results is that higher ligand densities are not always better. Gong *et al.* reported that polymeric micelles containing 10% folic acid (FA) (molar content) exhibited superior cytotoxicity and cellular uptake on ovarian cancer cell line OVCAR-3 in comparison to micelles with 50% and 91% FA.[35] Similarly, Yi *et al.* found that polymeric vesicles incorporating 2% transferrin (Tf) had higher cellular uptake and more remarkable ability to inhibit multidrug resistance (MDR) in tumor cells than those with 4% and 5% Tf.[36] Based on the literature review and the analysis of experimental findings, the uptake capacity of tumor cells for active targeting nanoparticles could be roughly divided into three distinct phases depending on the concentration of targeting ligands. During the initial phase, increasing concentration of targeting ligands resulted in greater uptake of micelles, because the interaction with specific receptors on the surface of cancer cells facilized internalization.[37,38] In the second stage, binding saturation was achieved at higher concentration of targeting ligands and there was no further enhancement in targeting ability. In the third phase, when the concentration continued to increase, the targeting ability of the nanoparticles was limited due to steric hindrance effects.[35,36,39] Therefore, there should be an optimal range for the

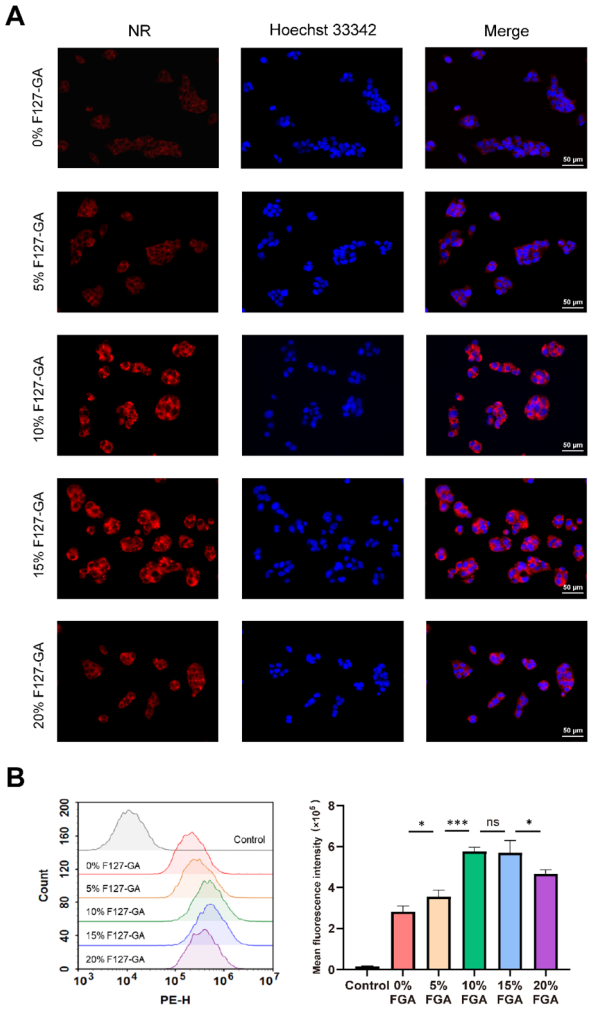

Fig. 5 (A) Fluorescence microscopy images of NR (red) intracellular uptake in HepG-2 cells after treatment with mixed micelles containing 0%, 5%, 10%, 15% and 20% F127-GA (FGA). Nuclei were labelled by Hoechst 33 342 (blue). The scale bar in the graph represented 50 μm. (B) Flow cytometry analysis and quantitation of the mean fluorescence intensity of HepG-2 cells treated with mixed micelles containing 0%, 5%, 10%, 15% and 20% F127-GA. Data were presented as mean ± SD; $n = 3$. *$P < 0.05$, ***$P < 0.001$ and ns $P > 0.05$.

concentration of the targeting ligands in nanoparticles to obtain greater targeting activity against tumor cells. Evaluating the density of targeting ligands in future research on active targeting drugs is essential.

It was reported that the redox-sensitivity of polymer mixed micelles tended to decrease when the proportion of reduction-sensitive polymeric materials was reduced.[38] Therefore, considering the active targeting function and the reduction sensitivity, we determined the optimal ratio of F127-GA : F127-SS-PDLA to be 10 : 90 in the mixed micelle. It could potentially enhance the efficiency and effectiveness of mixed micelles.

3.3 Characterization of CTD-loaded micelles

The particle size, PDI, zeta potential, DL and EE of various CTD-loaded micelles were listed in Table 1. The nanoparticles within the size range of 20–200 nm could not only take advantage of EPR effect to enhance the passive accumulation of drugs in tumor tissues, but also evade the phagocytosis by the reticulo-endothelial system (RES) and premature elimination through glomerular filtration.[40] Consequently, it was implied that CTD-loaded micelles would effectively aggregate in tumor sites. It was noteworthy that polymer mixed micelles GA/F127-SS-PDLA/CTD possessed smaller particle size (85.17 ± 1.24 nm) compared to F127-SS-PDLA/CTD micelles prepared from the single polymer material (102.20 ± 1.98 nm), which was also consistent with previous reports.[21] This preponderance of particle size would make polymer mixed micelles more likely to enter the tumor tissue through the EPR effect and be taken up by tumor cells.[41] The PDI value of GA/F127-SS-PDLA/CTD micelles was less than 0.200, which facilitating the micelles to cross the biological barrier effectively.[42] Moreover, GA/F127-SS-PDLA/CTD micelles had a zeta potential of −11.71 ± 0.86 mV which would contribute to improving hemocompatibility and prolonging the circulation time.[40]

Utilizing DLS to determine particle size and distribution has advantages of easy operation and fast analysis, but it cannot reflect the appearance and morphology of particles. Therefore, DLS and TEM are usually combined to comprehensively evaluate the nanoparticle from both quantitative and qualitative perspectives. As illustrated in Fig. 6A, the average particle sizes of GA/F127-SS-PDLA/CTD and F127-SS-PDLA/CTD micelles were about 72 and 89 nm, respectively. They possessed uniform spherical structure with good dispersion and no fragmentation, adhesion or aggregation. The particle sizes observed by TEM were smaller than those measured *via* DLS, which was attributed to the drying and tightening of micelles during sample preparation.[38]

3.4 The stability of CTD-loaded micelles

The stability of nanoparticles is not only beneficial for drug transport and storage, but also for the anti-tumor effect of drug.[25,43] As displayed in Fig. 6D, when stored at 4 °C for 30 days, negligible variations of particle size and PDI were observed in F127-SS-PDLA/CTD and GA/F127-SS-PDLA/CTD micelles. It was

Table 1 Characterization of different CTD-loaded micelles (mean ± SD; $n = 3$)

Micelles	Size (nm)	Polydispersity	Zate potential (mV)	Encapsulation efficiency (%)	Drug loading (%)
F127-PDLA/CTD	114.55 ± 2.09	0.102 ± 0.015	−8.47 ± 0.33	93.25 ± 1.51	15.72 ± 0.22
F127-SS-PDLA/CTD	102.20 ± 1.98	0.141 ± 0.010	−10.08 ± 0.41	95.37 ± 0.93	16.02 ± 0.13
GA/F127-SS-PDLA/CTD	85.17 ± 1.24	0.132 ± 0.005	−11.71 ± 0.86	96.09 ± 0.81	16.12 ± 0.11

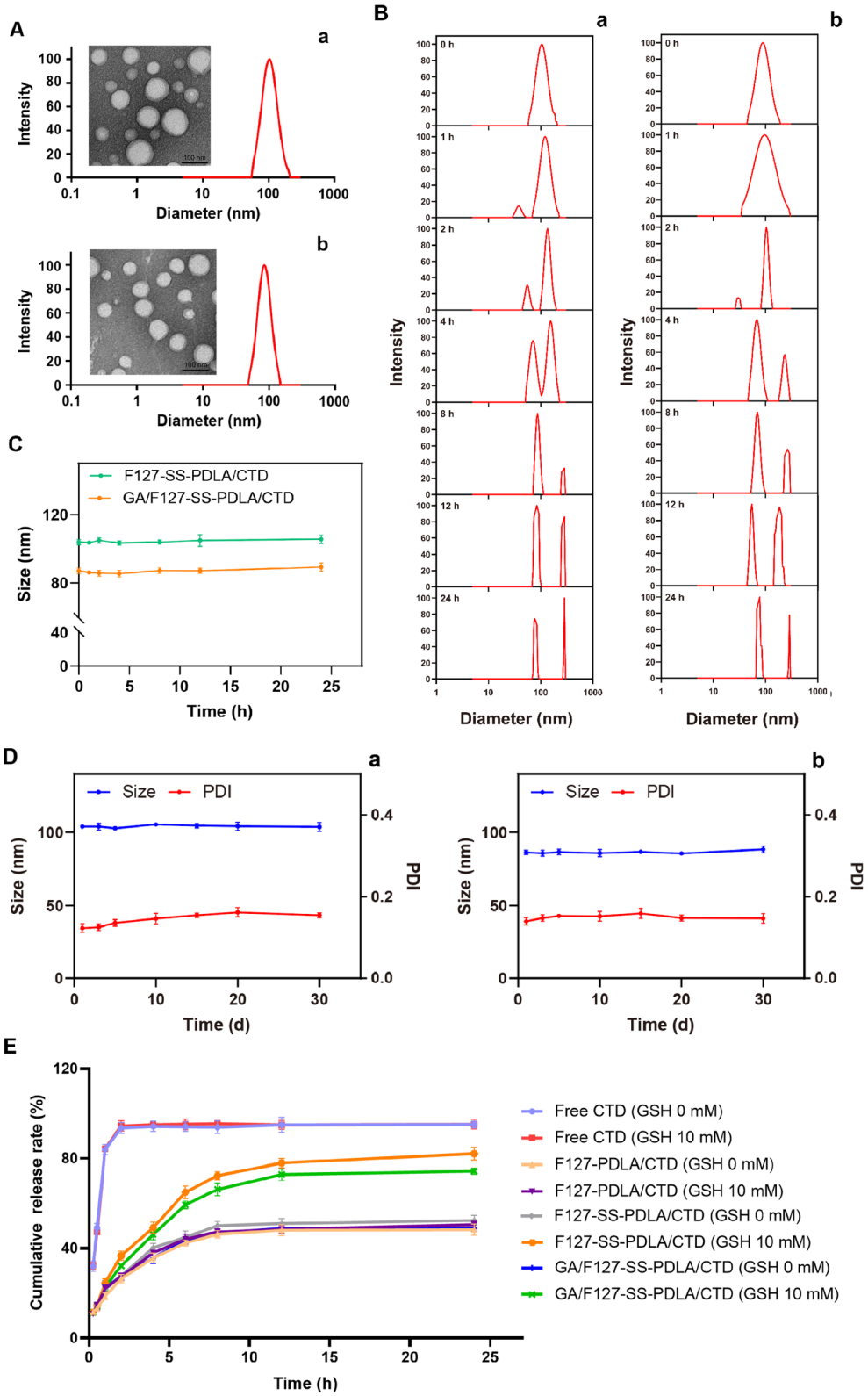

Fig. 6 (A) Size distribution and morphology of F127-SS-PDLA/CTD (a) and GA/F127-SS-PDLA/CTD (b) micelles detected with DLS and TEM. The scale bar for TEM represents 100 nm. (B) Size distributions of F127-SS-PDLA/CTD (a) and GA/F127-SS-PDLA/CTD (b) micelles under reductive environment (10 mM GSH) for 24 h. (C) Changes in particle size of CTD-loaded micelles incubated with 10% FBS at 37 °C for 24 h. (D) Changes in particle size and PDI of F127-SS-PDLA/CTD (a) and GA/F127-SS-PDLA/CTD (b) micelles stored at 4 °C for 30 days. (E) Cumulative release profiles of free CTD and CTD in CTD-loaded micelles in normal saline with different GSH concentrations (0 and 10 mM). Data were presented as mean ± SD; $n = 3$.

manifested that CTD-loaded micelles had excellent capacity for long-term storage, which was possibly contributed to the negative charge on the surface of the micelles.[41]

When entering the physiological environment, nanoparticles could be coated with biomacromolecules in the blood such as proteins, which might lead to aggregation and precipitation.[44,45] As shown in Fig. 6C, F127-SS-PDLA/CTD and GA/F127-SS-PDLA/CTD micelles were basically stable in 10% FBS within 24 h with little changes in particle size, indicating that the protein adsorbed on the surface of the micelles was less and CTD-loaded micelles possessed the potential to remain stable in blood circulation.

3.5 Reduction-responsive behaviour of CTD-loaded micelles

The disulfide bonds between F127 and PDLA made micelles susceptible to redox environment. The changes in size distribution of F127-SS-PDLA/CTD and GA/F127-SS-PDLA/CTD micelles in 10 mM GSH were monitored by DLS. As illustrated in Fig. 6B, the particle size of the micelles showed a pronounced bimodal distribution starting from 4 h in 10 mM GSH. Moreover, with the increase of time, the signal intensity of larger particle size increased continuously. It could be inferred that F127-SS-PDLA/CTD and GA/F127-SS-PDLA/CTD micelles were gradually decomposed to release drugs in the reducing environment. The results were similar to the previous study. Liu *et al.* reported that significant changes in particle size distribution and morphology of the redox-sensitive micelles were observed under reductive conditions.[26] The main reason was that the cleavage of the disulfide bonds connecting F127 and PDLA resulted in the disruption of the micelle structure, the aggregation of hydrophobic chain segments and the formation of larger particles.[24,25]

3.6 *In vitro* drug release

In vitro cumulative release assay is usually used to estimate the drug release rate and the total amount, which is one of the evaluation methods for sustained and controlled-release formulations.[46] The drug release behaviors of free CTD and three CTD-loaded micelles were investigated in different release media by the dialysis method. As illustrated in Fig. 6E, free CTD showed a burst release characteristic with approximately 90% CTD were released within 2 h whatever the concentrations of GSH. In contrast, CTD-loaded micelles all exhibited sustained release pattern. The release trend of CTD from F127-PDLA/CTD micelles was roughly the same whatever in normal saline or 10 mM GSH, indicating that the non-sensitive micelles could maintain stability in the reductive environment. The cumulative release rates of F127-SS-PDLA/CTD and GA/F127-SS-PDLA/CTD micelles in normal saline were 52.35 ± 2.33% and 48.89 ± 1.44% within 24 h, while CTD released from F127-SS-PDLA/CTD and GA/F127-SS-PDLA/CTD micelles reached 82.10 ± 2.91% and 74.36 ± 1.46% respectively in 10 mM GSH solution. It was related to the hydrolysis and fracture of disulfide bonds, leading to the rapid release of drugs. These results revealed that F127-SS-PDLA conjugate was able to achieve redox-responsive drug release in tumor cells and maintain stability in normal physiological environment, which was of great value for treating cancer and protecting normal cells.

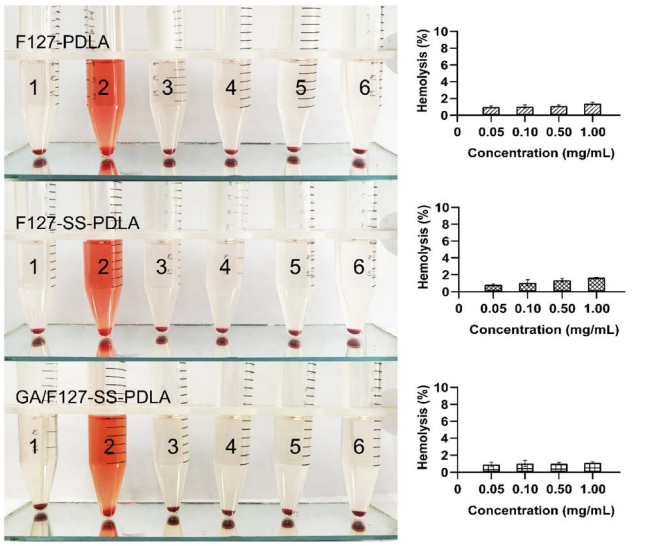

Fig. 7 The hemolysis situation of blank F127-PDLA, F127-SS-PDLA and GA/F127-SS-PDLA micelles in different concentrations. The bar charts of hemolysis rates of blank micelles in various concentrations. Sample 1 represented negative control; sample 2 represented positive control; samples 3, 4, 5 and 6 represented blank micelles at the concentrations of 0.05, 0.10, 0.50, and 1.00 mg mL^{-1}, respectively. Data were presented as mean ± SD; $n = 3$.

3.7 Hemolysis assay

In order to validate the safety of polymer materials, their blood compatibility should be evaluated through a hemolysis assay. As could be seen from Fig. 7, three blank micelles F127-PDLA, F127-SS-PDLA and GA/F127-SS-PDLA exhibited no significant hemolysis even at 1.00 mg mL^{-1}. The American Society for Testing and Materials (ASTM) classified materials into three grades according to their degrees of hemolysis: hemolytic (hemolysis rate greater than 5%), mildly hemolytic (hemolysis rate 2–5%) and non-hemolytic (hemolysis rate less than 2%).[26,47] The hemolysis rates of the three materials were all less than 2% in the concentration range of 0.50–1.00 mg mL^{-1}, reflecting that F127-PDLA, F127-SS-PDLA and GA/F127-SS-PDLA micelles possessed great blood compatibility within the experimental concentration range and could meet the requirements of intravenous injection.

3.8 Cytotoxicity assay

MTT assay were performed on HepG-2 cells to study the cytotoxicity of CTD-loading micelles. In order to further investigate the biocompatibility of carrier materials, the cytotoxicity of blank micelles F127-PDLA, F127-SS-PDLA and GA/F127-SS-PDLA was firstly tested. As illustrated in Fig. 8C, after incubation for 24 h, no significant inhibition of the blank micelles was found on the growth of HepG-2 cells in the concentration range of 3.125–200 μg mL^{-1} (cellular viability was all above 85%), manifesting that they had great biocompatibility within the

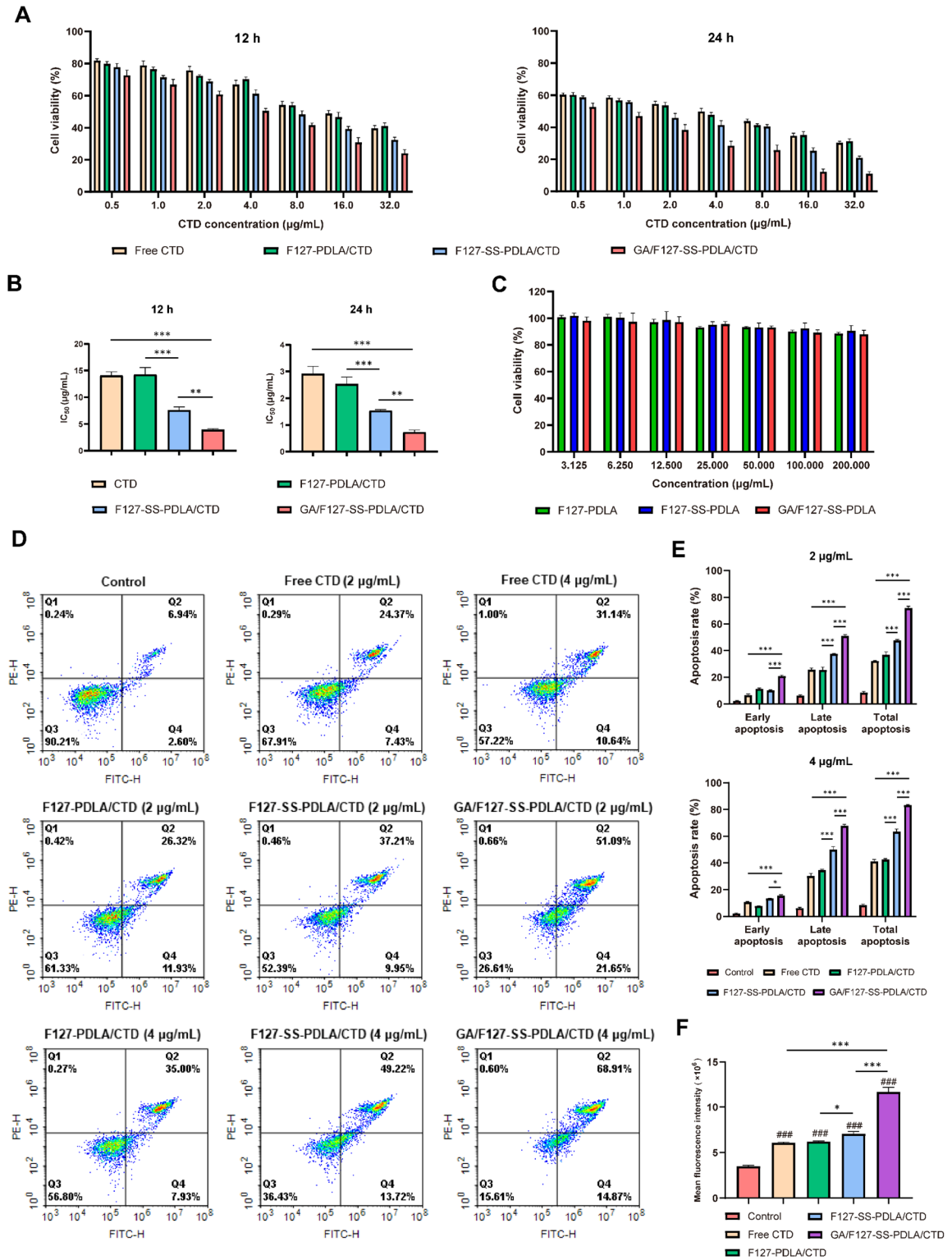

Fig. 8 (A) Cytotoxicity of various CTD formulations against HepG-2 cells for 12 h and 24 h. (B) IC_{50} values of free CTD and CTD-loaded micelles. (C) Cell viability of HepG-2 cells incubated with the different concentrations of three blank micelles for 24 h. (D) Representative scatter plots of Annexin V/PI analysis of HepG-2 cells treated with different concentrations of drugs for 12 h. (E) Percentage of HepG-2 cells with early, late and complete apoptosis after treatment with different concentrations of drugs. (F) Quantitation of the mean fluorescence intensity measurement of intracellular ROS levels of HepG-2 cells treated with free CTD and CTD-loaded micelles. Data were presented as mean ± SD; $n = 3$. $^{*}P < 0.05$, $^{**}P < 0.01$, $^{***}P < 0.001$ and $^{\#\#\#}P < 0.001$ *vs.* control.

Table 2 The IC_{50} values of HepG-2 cells treated with free CTD, F127-PDLA/CTD, F127-SS-PDLA/CTD and GA/F127-SS-PDLA/CTD micelles for 12 h and 24 h (mean ± SD; $n = 3$)

	IC_{50} (μg mL^{-1})			
Time (h)	Free CTD	F127-PDLA/CTD	F127-SS-PDLA/CTD	GA/F127-SS-PDLA/CTD
12	14.08 ± 0.70	14.26 ± 1.32	7.631 ± 0.601	3.924 ± 0.210
24	2.917 ± 0.274	2.527 ± 0.263	1.545 ± 0.036	0.7315 ± 0.0791

range of certain concentration and would exert no influence on the outcomes of subsequent experiments.

As showcased in Fig. 8A, when treatment period and concentration of CTD increased, the inhibitory effects of free CTD and CTD-loaded micelles on the growth of tumor cells were enhanced, which exhibited a time and concentration-dependent manner. The half maximal inhibitory concentration (IC_{50}) values of free CTD and CTD-loaded micelles were illustrated in Table 2 and summarized in Fig. 8B. The IC_{50} value of F127-SS-PDLA/CTD micelles was significantly lower than those of F127-PDLA/CTD micelles and free CTD ($P < 0.001$). This suggested that redox-sensitive micelles were able to rapidly release drugs in response to the intracellular redox environment, and therefore the equivalent inhibitory effect could be achieved at lower concentration of CTD. Furthermore, GA/F127-SS-PDLA/CTD micelles displayed the strongest inhibition ability, whose IC_{50} was about 1/2 of that of F127-SS-PDLA/CTD micelles. It was probably resulted from the specific interaction between GA and the GA receptor on the surface of HepG-2 cells, which enhanced the internalization of GA/F127-SS-PDLA/CTD micelles and increased drug accumulation.

3.9 Apoptosis assay

To further confirm whether the inhibitory effect of GA/F127-SS-PDLA/CTD micelles on HepG-2 cell was connected with the induction of apoptosis, we performed apoptosis assay *via* the mothed of Annexin V/PI double staining. As shown in Fig. 8D and E, compared with the control group, treatment with 2 μg mL^{-1} and 4 μg mL^{-1} of free CTD, F127-PDLA/CTD, F127-SS-PDLA/CTD and GA/F127-SS-PDLA/CTD micelles for 12 h significantly enhanced the population of apoptotic cells. Furthermore, the concentration of drug had a significant impact on apoptosis rate ($P < 0.05$). At the concentration of 2 μg mL^{-1} and 4 μg mL^{-1}, the total apoptosis rates of GA/F127-SS-PDLA/CTD group were 71.86 ± 1.44% and 83.25 ± 0.46%, respectively, which were 2.23 and 2.03 times higher than those of free CTD group, 1.95 and 1.96 times higher than those of F127-PDLA/CTD group, 1.51 and 1.31 times higher than those of F127-SS-PDLA/CTD group. The redox-sensitive F127-SS-PDLA/CTD micelles demonstrated higher late and total apoptotic rates than the non-sensitive F127-PDLA/CTD micelles.

However, F127-SS-PDLA/CTD micelles displayed lower early apoptotic rate at 2 μg mL^{-1}. This discrepancy might be attributed to the rapid release of CTD by redox-sensitive micelles in response to intracellular high concentrations of GSH, which directly induce the tumor cells into the late apoptotic state, and therefore the proportion of cells in early apoptosis was reduced. Notably, GA/F127-SS-PDLA/CTD micelles had significantly higher early, late and total apoptosis rates than other groups no matter what the concentration was. In conclusion, GA/F127-SS-PDLA/CTD micelles were more efficient than other preparations in targeting HepG-2 cells and releasing CTD to induce apoptosis of cells.

3.10 Intracellular ROS levels

Intracellular ROS, a by-product of cellular oxygen consumption and metabolism, is closely related to apoptosis and death of tumor cells.[48–50] Studies have demonstrated that CTD was able to induce apoptosis in a variety of tumor cells by increasing the levels of intracellular ROS.[9,51] Therefore, the generation of ROS in HepG-2 after drug treatment were evaluated *via* DCFH-DA staining to explore the relationship between ROS and the cytotoxicity. As shown in Fig. 8F, after treatment with free CTD, F127-PDLA/CTD, F127-SS-PDLA/CTD and GA/F127-SS-PDLA/CTD micelles, the generation of ROS in HepG-2 cells was significantly increased. The ROS levels of different groups in HepG-2 cells were in the order of GA/F127-SS-PDLA/CTD micelles > F127-SS-PDLA/CTD micelles > F127-PDLA/CTD micelles ≈ free CTD > control. These results manifested that GA/F127-SS-PDLA/CTD micelles were able to augment intracellular ROS levels through GA receptor-mediated endocytosis and reduction sensitive function. However, the F127-PDLA/CTD micelles group showed no significant disparity compared to the free CTD group, possibly attributed to its slow drug release and lack of active targeting function. Combined with the results above, it was indicated that CTD could upregulate intracellular ROS levels, induce cellular apoptosis, and ultimately cause cell death. Moreover, GA/F127-SS-PDLA/CTD micelles could reinforce this process to some extent.

3.11 Cellular uptake assay

The intracellular uptake ability of F127-PDLA/NR, F127-SS-PDLA/NR and GA/F127-SS-PDLA/NR by HepG-2 cells was observed and imaged by fluorescent microscope. As displayed in Fig. 9A, it could be clearly observed that NR (red fluorescence) and Hoechst 33 342 (blue fluorescence) were mainly distributed in the cytoplasts and nuclei, respectively. After administration for 4 h, the order of the red fluorescence intensity in HepG-2 cells was as following: GA/F127-SS-PDLA/NR micelles > F127-SS-PDLA/NR micelles > F127-PDLA/NR micelles. Fluorescence intensity of cells was further measured by flow cytometry to quantify the uptake efficiency of various micelles (Fig. 9B). After cultured with F127-SS-PDLA/NR micelles for 4 h, the mean fluorescence intensity in HepG-2 cells was 1.5 times higher than

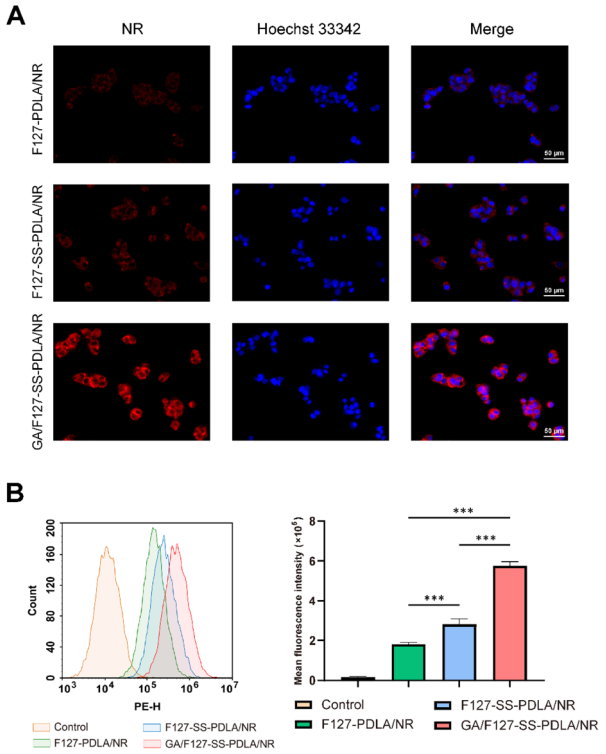

Fig. 9 (A) Fluorescence microscopy images of NR (red) intracellular uptake in HepG2 cells after treatment with F127-PDLA/NR, F127-SS-PDLA/NR and GA/F127-SS-PDLA/NR micelles. Nuclei were labelled by Hoechst 33 342 (blue). The scale bar in the graph represented 50 μm. (B) Flow cytometry analysis and quantitation of the mean fluorescence intensity of HepG-2 cells treated with NR-loaded micelles. Data were presented as mean ± SD; $n = 3$. ***$P < 0.001$.

that in F127-PDLA/NR micelles group. Furthermore, the mean fluorescence intensity of GA/F127-SS-PDLA/NR group was 2.0 and 3.2 times higher than those of F127-SS-PDLA/NR and F127-PDLA/NR groups, respectively. This indicated that the release of NR from micelles was promoted by the high GSH concentration in HepG-2 cells, bringing about stronger intracellular fluorescence intensity of reduction-sensitive micelles group compared with non-sensitive micelles group. Similar results were observed in previous.[22,52,53] We speculated that those fluorescent substances that had not been released seem to be covered with a "thin film", so the fluorescence intensity was slightly weaker. Meanwhile, the uptake of GA/F127-SS-PDLA/NR micelles was higher than that of F127-SS-PDLA/NR and F127-PDLA/NR micelles. The results further manifested that the modification of GA could promote the selective uptake of micelles *via* GA receptor-mediated endocytosis by HepG-2 cells.

4 Conclusions

Nano-drug delivery systems can address the problems on poor water solubility, strong toxic and side effects and inadequate targeting ability of anti-tumor ingredients in traditional Chinese medicines. However, due to the intricate tumor microenvironment, drug delivery systems with single-function alone are insufficient to provide effective treatment. In this study, we designed and developed CTD-loaded polymeric mixed micelles GA/F127-SS-PDLA/CTD with active targeting and redox-sensitive functions for HCC therapy. GA/F127-SS-PDLA/CTD micelles exhibited uniform particle size distribution, spherical morphology, excellent stability and biocompatibility, as well as demonstrated exceptional drug-loading ability for CTD and reduction-responsive drug release characteristic. *In vitro* drug release assay manifested that GA/F127-SS-PDLA/CTD micelles could remain stable under physiological conditions and release rapidly under high GSH conditions. In cytological experiments showed that the anti-tumor ability of reduced sensitive micelles F127-SS-PDLA/CTD was stronger than that of non-sensitive micelles F127-PDLA/CTD, because in response to the intracellular reductive environment, F127-SS-PDLA/CTD micelles were able to release drugs rapidly in tumor cells, and thereby inhibit proliferation and enhance apoptosis. Meanwhile, GA/F127-SS-PDLA/CTD micelles exhibited the most effective cytotoxicity, apoptosis, elevation of ROS level and cellular uptake in HepG-2 cells, since GA/F127-SS-PDLA/CTD micelles had both reduction sensitivity and active targeting function. They could effectively recognize the GA receptor on the surface of tumor cells and promote internalization of micelles. Last but not least, it was found that the targeting ability of GA/F127-SS-PDLA/CTD micelles with 10% and 15% F127-GA was better than those with 5% and 20% F127-GA. Therefore, the density of targeting ligands was not necessarily higher, but should have an optimal range. In conclusion, this novel drug delivery system has the potential to compensate for the insufficient targeting ability of the current CTD preparations, and thereby further enhancing its anti-tumor efficacy.

Data availability

The data that support the findings of this study are available from the corresponding author upon reasonable request.

Conflicts of interest

There are no conflicts to declare.

Acknowledgements

This research was funded by Strengthening Foundation Plan for Young Teachers of School of Pharmacy, Shandong University of Traditional Chinese Medicine (SDTCM) (No. KYQJ-202314), the project of High-Level Traditional Chinese Medicine Key Disciplines of the State Administration of Traditional Chinese Medicine and the National Science Foundation for Distinguished Young Scholars of China and National Natural Science Foundation of China (Youth Program) (Grant No. 82305051). All authors gratefully acknowledge Dr Jing Sun, Dr Zhenhua Tian and Dr Shuai Man from Chinese Experimental Centre for laboratory equipment of SDTCM for their guidance of HPLC, ^{1}H-NMR and FTIR studies. All the authors thank National Centre for Protein Sciences at Peking University in Beijing, China, for its guidance on TEM.

References

1 E. Chakraborty and D. Sarkar, *Cancers*, 2022, **14**, 151–172.
2 S. Lu, J. Huang, J. Zhang, C. Wu, Z. Huang, X. Tao, L. You, A. Stalin, M. Chen, J. Li, Y. Tan, Z. Wu, L. Geng, Z. Li, Q. Fan, P. Liu, Y. Lin, C. Zhao and J. Wu, *J. Ethnopharmacol.*, 2024, **319**, 117209.
3 M. Zou, Y. Xu, P. Lin, L. Zhou and X. Xia, *J. Liposome Res.*, 2023, **33**, 1–17.
4 M. Ibrahim, W. H. Abuwatfa, N. S. Awad, R. Sabouni and G. A. Husseini, *Pharmaceutics*, 2022, **14**, 254.
5 H. Yao, J. Zhao, Z. Wang, J. Lv, G. Du, Y. Jin, Y. Zhang, S. Song and G. Han, *Colloids Surf., B*, 2020, **196**, 111285.
6 F. Naz, Y. Wu, N. Zhang, Z. Yang and C. Yu, *Molecules*, 2020, **25**, 3279.
7 S. Hu, J. Chang, H. Ruan, W. Zhi, X. Wang, F. Zhao, X. Ma, X. Sun, Q. Liang, H. Xu, Y. Wang and Y. Yang, *Int. J. Biol. Sci.*, 2021, **17**, 2504–2522.
8 Y. Pan, Q. Zheng, W. Ni, Z. Wei, S. Yu, Q. Jia, M. Wang, A. Wang, W. Chen and Y. Lu, *Front. Pharmacol*, 2019, **10**, 590.
9 W. Huang, S. Ko, H. Tsai, J. Chung, J. Chiang, K. Chen, Y. Chen, H. Chen, Y. Chen and J. Yang, *Int. J. Oncol.*, 2011, **38**, 1067–1073.
10 K. Zhu, L. Zhou, M. Zou, S. Ning, S. Liu, Y. Zhou, K. Du, X. Zhang and X. Xia, *J. Pharm. Sci.*, 2020, **109**, 2038–2047.
11 B. Zhai, J. Sun, Y. Shi, X. Zhang, J. Zou, J. Cheng, Y. Fan, D. Guo and H. Tian, *J. Nanobiotechnol.*, 2022, **20**, 509.
12 P. An, D. Lu, L. Zhang, H. Lan, H. Yang, G. Ge, W. Liu, W. Shen, X. Ding, D. Tang, W. Zhang, X. Luan, H. Cheng and H. Zhang, *Phytomedicine*, 2022, **103**, 154231.
13 X. Liu, L. Zhang, W. Tang, T. Zhang, P. Xiang, Q. Shen, T. Ye and Y. Xiao, *Toxicol. Appl. Pharmacol.*, 2023, **465**, 116450.
14 W. Cheng, Y. Wang, J. Liu, X. Li, M. Yu, C. Duan, L. Liu and J. Zhang, *J. Appl. Toxicol.*, 2021, **42**, 970–980.
15 D. Jin, N.-N. Huang and J.-X. Wei, *Front. Pharmacol*, 2023, **14**, 1201404.
16 J. Wu, *J. Pers. Med.*, 2021, **11**, 771.
17 I. D. Zlotnikov, D. A. Streltsov, A. A. Ezhov and E. V. Kudryashova, *Pharmaceutics*, 2023, **15**, 1135.
18 D. Hwang, J. D. Ramsey and A. V. Kabanov, *Adv. Drug Delivery Rev.*, 2020, **156**, 80–118.
19 H. Cabral and K. Kataoka, *J. Controlled Release*, 2014, **190**, 465–476.
20 X.-B. Fang, J.-M. Zhang, X. Xie, D. Liu, C.-W. He, J.-B. Wan and M.-W. Chen, *Int. J. Pharm.*, 2016, **502**, 28–37.
21 J. Song, Y. Liu, L. Lin, Y. Zhao, X. Wang, M. Zhong, T. Xie, Y. Luo, S. Li, R. Yang and H. Li, *RSC Adv.*, 2019, **9**, 40131–40145.
22 C. Tian, S. Asghar, Z. Hu, Y. Qiu, J. Zhang, F. Shao and Y. Xiao, *Int. J. Biol. Macromol.*, 2019, **136**, 143–153.
23 X. Du, S. Yin, F. Zhou, X. Du, J. Xu, X. Gu, G. Wang and J. Li, *Int. J. Pharm.*, 2018, **550**, 1–13.
24 L. Zou, X. Liu, J. Li, W. Li, L. Zhang, C. Fu, J. Zhang and Z. Gu, *Theranostics*, 2021, **11**, 4171–4186.
25 Y. Yuan, Z. Wang, S. Su, Y. Mi, Q. Li, F. Dong, W. Tan and Z. Guo, *Int. J. Biol. Macromol.*, 2023, **247**, 125849.
26 Y. Liu, S. Fu, L. Lin, Y. Cao, X. Xie, H. Yu, M. Chen and H. Li, *Int. J. Nanomed.*, 2017, **12**, 2635–2644.
27 P. Dehghan Kelishady, E. Saadat, F. Ravar, H. Akbari and F. Dorkoosh, *Pharm. Dev. Technol.*, 2014, **20**, 1009–1017.
28 P. S. Giram, J. T.-W. Wang, A. A. Walters, P. P. Rade, M. Akhtar, S. Han, F. N. Faruqu, H. M. Abdel-Bar, B. Garnaik and K. T. Al-Jamal, *Biomater. Sci.*, 2021, **9**, 795–806.
29 Y. Shi, R. van der Meel, X. Chen and T. Lammers, *Theranostics*, 2020, **10**, 7921–7924.
30 Z. Li, X. Xiong, S. Peng, X. Chen, W. Liu and C. Liu, *J. Microencapsulation*, 2020, **37**, 220–229.
31 A. A. Shitole, N. Sharma, P. Giram, A. Khandwekar, M. Baruah, B. Garnaik and S. Koratkar, *Mater. Sci. Eng. C*, 2020, **114**, 111035.
32 F. Wu, X. Li, B. Jiang, J. Yan, Z. Zhang, J. Qin, W. Yu and Z. Gao, *J. Biomed. Nanotechnol.*, 2018, **14**, 1837–1852.
33 C. T. Dinh, H. T. Vu, Q. T. H. Phan, L. P. Nguyen, T. Q. Tran, D. Van Tran, N. N. Quy, D. T. N. Pham and D. T. Nguyen, *J. Mater. Sci.: Mater. Med.*, 2022, **33**, 72.
34 Y. Hu, J. Song, A. Feng, J. Li, M. Li, Y. Shi, W. Sun and L. Li, *Molecules*, 2023, **28**, 7767.
35 Y. C. Gong, X. Y. Xiong, X. J. Ge, Z. L. Li and Y. P. Li, *Macromol. Biosci.*, 2019, **19**, e1800348.
36 S. L. Yi, Z. L. Li, Y. C. Gong and X. Y. Xiong, *Langmuir*, 2023, **39**, 15920–15931.
37 M. K. Riaz, X. Zhang, K. H. Wong, H. Chen, Q. Liu, X. Chen, G. Zhang, A. Lu and Z. Yang, *Int. J. Nanomed.*, 2019, **14**, 2879–2902.
38 Y. Zhong, W. Yang, H. Sun, R. Cheng, F. Meng, C. Deng and Z. Zhong, *Biomacromolecules*, 2013, **14**, 3723–3730.
39 A. Grigoletto, G. Martinez, D. Gabbia, T. Tedeschini, M. Scaffidi, S. Martin and G. Pasut, *Pharmaceutics*, 2021, **13**, 929.
40 J. Liu, N. Liang, S. Li, Y. Han, P. Yan, Y. Kawashima, F. Cui and S. Sun, *J. Biomater. Appl.*, 2020, **34**, 1458–1469.
41 N. S. Noor, N. H. M. Kaus, M. R. Szewczuk and S. B. S. Hamid, *Int. J. Mol. Sci.*, 2021, **22**, 9420.
42 X. P. Chen, Y. Li, Y. Zhang and G. W. Li, *Drug Des., Dev. Ther.*, 2019, **13**, 3569–3578.
43 Y. Liu and X. An, *Colloids Surf., B*, 2019, **178**, 238–244.
44 L. Yu, M. Xu, W. Xu, W. Xiao, X. H. Jiang, L. Wang and H. Gao, *Nano Lett.*, 2020, **20**, 8903–8911.
45 L. Rao, Q. F. Meng, L. L. Bu, B. Cai, Q. Huang, Z. J. Sun, W. F. Zhang, A. Li, S. S. Guo, W. Liu, T. H. Wang and X. Z. Zhao, *ACS Appl. Mater. Interfaces*, 2017, **9**, 2159–2168.
46 W. Jiang, J. Guo, W. Wen, Y.-G. Jia and S. Liu, *Materials*, 2019, **12**, 1610.
47 F. K. Andrade, J. P. Silva, M. Carvalho, E. M. S. Castanheira, R. Soares and M. Gama, *J. Biomed. Mater. Res., Part A*, 2011, **98A**, 554–566.
48 J. Liu, Y. Xu, H. Lu, R. Wang, Z. Xia, C. Zhao, D. Huang, F. Jiang and W. Chen, *Langmuir*, 2022, **38**, 13955–13962.
49 B. Ren, Z.-C. Cai, X.-J. Zhao, L.-S. Li and M.-X. Zhao, *Int. J. Nanomed.*, 2021, **16**, 7023–7033.
50 S. Vafaei, S. A. Sadat Shandiz and Z. Piravar, *Biol. Trace Elem. Res.*, 2020, **198**, 109–117.

51 T. C. Hsia, C. C. Yu, S. C. Hsu, N. Y. Tang, H. F. Lu, Y. P. Huang, S.-H. Wu, J.-G. Lin and J.-G. Chung, *Int. J. Oncol.*, 2014, **45**, 245–254.
52 L. Han, L. Hu, F. Liu, X. Wang, X. Huang, B. Liu, F. Feng, W. Liu and W. Qu, *Asian J. Pharm. Sci.*, 2019, **14**, 531–542.
53 M. Huo, Y. Liu, L. Wang, T. Yin, C. Qin, Y. Xiao, L. Yin, J. Liu and J. Zhou, *Mol. Pharm.*, 2016, **13**, 1750–1762.